Particle migration in deformable channels coupled with the Fåhræus-Lindqvist effect

Thesis submitted to the Indian Institute of Technology Kharagpur

in partial fulfillment of the requirements of the degree

of

Bachelor of Technology (Hons.) in Mechanical Engineering

by

Aniruddha Saha (17ME10075)

under the supervision of

Dr. Jeevanjyoti Chakraborty

Department of Mechanical Engineering
Indian Institute of Technology Kharagpur

April 2021

Certificate

This is to certify that the thesis entitled **Particle migration in deformable channels coupled with the Fåhræus-Lindqvist effect**, submitted by **Aniruddha Saha** (roll number. **17ME10075**) to the Indian Institute of Technology Kharagpur, is a record of bona fide research work under my supervision and I consider it worthy of consideration for the award of the degree of **B. Tech (Hons.)** in **Mechanical Engineering** of the Institute.

Dr.Jeevanjyoti Chakraborty
Department of Mechanical Engineering
Indian Institute of Technology Kharagpur
Kharagpur-721302,India

Date:

Acknowledgements

I take this opportunity to express my gratitude and regards to my guide, Dr. Jeevanjyoti Chakraborty, Assistant Professor, Department of Mechanical Engineering, Indian Institute of Technology Kharagpur, for his awesome guidance and encouragement. I am indebted to Pratyaksh Karan, PhD scholar, Department of Mechanical Engineering, Indian Institute of Technology Kharagpur, for his insights and ideas. This project would not have been in its current form without their help throughout the period and more significantly, during setbacks. It shall always be an indelible experience to work with such amazing people.

—**Aniruddha Saha**

IIT Kharagpur

Abstract

We present a study on the Fåhræus-Lindqvist effect in controlling particle migration in deformable channels. The response of fluid pressure driving the flow manifests into wall deformation, and the flow is governed by the Giesekus constitutive relation. The superposition of the contributions to migration from elastic forces and non-uniform channel geometry lead onto a variety of particle distribution with precise control. The tendency of the deformed channel to enhance migration has been captured well by the effect of a Newtonian layer formation that inhibits lateral movement of particles in the localised region. The complex interplay of such an effect along with the wall deformability in modulating the particle motion is reaffirmed by a particle distribution function constructed for theoretical neutrally buoyant particles over an array of flow tuning parameters.

Contents

List of Figures

Introduction

Blood flow in the human body is an integral part of the study on non-Newtonian fluids. As the flow occurs from a large vessel to a small-diameter one, the hematocrit level decreases as first proposed in [3]. A decrease in the apparent viscosity as the vessel diameter decreases also occurs [4]. Such an effect is accompanied with more diverse subtleties considering the deformability of the blood vessel. The most driving forces behind such flows is a pressure gradient applied across the channel ends. Among such flows, we give special importance to the Hagen-Poiseuille flow in cylindrical micro-channels in this study. We consider a fluid whose stresses obey the power law, and flows through a channel having deformable walls. As microfluidics gradually developed, flow in micro-channels became predominantly important. Of particular importance is the use of microfluidics to model and simulate complex liquid flow such as blood through blood vessels. An important aspect of such biological flows is the presence of suspended molecules in them that travel along the flow and sometimes are paramount to the paradigm of drug delivery [5]. The migration of red blood cells in microchannels has been addressed in 2D, and 3D geometries in [6] and [7], respectively; numerous RBCs are considered considering the deformation of the cells.

We build upon a generalised Hagen-Poiseuille flow where the channel walls are not rigid and introduce spherical neutrally buoyant particles and understand the dynamics. An annular region forms wherein the flow of the complex fluid occurs in the core region. The formation of a plasma layer on the perimeter is assumed to be of Newtonian nature. The boundaries of the channel deform as a result of the flow. The incorporation of the

deformability and the elastic nature of the flow gives imparts a new aspect to the trajectory of the suspended particles. Manipulation of small-scale particles, such as submicron colloidal particles and macromolecules is accompanied with numerous difficulties. Lateral migration velocity primarily depends upon the viscoelastic nature of the flow that is captured by the Weissenberg number and the aspect ratio of particle size to channel height [8].

The forces responsible for the displacement of a particle in a Poiseuille flow were proposed to be of inertial origin [9, 10]when the rheology of non-Newtonian fluids wasn't fully understood. The similarity between such migrations in suspensions and in biological fluids were observed [11], and this has led to the applications in biomimetic platforms where particles could be focused using the elasticity of a DNA based fluid where the effect of polymer viscosity was prominent [12] and plasma-based viscoelastic solutions [13]. Numerical simulations of such biomimetic applications have been done [14] where channel geometry and solution concentration have important effects on the phenomenon. Focusing in shear-thinning and Newtonian fluids have been studied for rectangular and square channels for axial flow [15], and we see the distinct equilibrium position of the suspended particles. Microchannels based on porosity, resistance to flow have been constructed in [16], and particle migration has been studied therein. Such tuning of displacements was reported in [17] giving importance to the rheological properties of the solvent which can be tuned for controlled focusing. Particle sorting became an important application as the migration was sensitive to the radius of these suspended spheres. Double-line sorting was observed for fluid with negative normal stress difference [18] and applied for a binary and ternary particle mixture in a visco-elastic fluid [19]. Square channels specifically exhibit interesting migration patterns [15, 20], and we see in [20] how the competition between inertial and elastic forces determines the occurrence of a single stream of particles, which tend to get scattered otherwise. Such deviations are numerically studied for a Newtonian fluid, [21] where the particles were displaced towards the channel axis with equilibrium

points on the axis. Such points became unstable as the elastic forces increased. In [22] the effect of a non-zero second normal stress difference is studied for non-Newtonian fluid suspensions. The deformability of the particles has been studied in Newtonian fluid suspensions [23], which showed how the force that is initially negative and pushes the particle towards the wall becomes positive later and allows the particle to attain an equilibrium position. In [24], we see the tendency of particle displacement due to normal stresses and channel geometry towards the closest wall due to instabilities contrary to the case of Newtonian liquids with inertial forces. [17].

The presence of an annular peripheral region of a Newtonian fluid, eliminates the development of first and second normal stresses that affect the migration of particles in the region. Different fluid models are able to capture certain aspects of flow behaviour, and the Giesekus model [25] is an advanced constitutive relation that introduces a non-linear mobility parameter [26], α. Two other fundamental parameters that define the model are - relaxation time λ, which captures the fluid elasticity and η, the zero shear viscosity. D'Avino et al. [1] analysed particle migration in circular channels using a Giesekus fluid, with the intended application of particle migration in flow focusing in microchannels. Romeo et al. [2] carried out similar investigations primarily based on a scaling that that unifies the migration characteristics over a range of flow parameters. New methods are being developed to control the displacements of these suspended particles as well as droplets [27], and we introduce a novel way by incorporating deformation in the channel walls, which have significant consequences on the particle distribution function (PDF) along the forces arising from the normal stress difference gradients.

Modelling of the Physical System

We model a pressure-driven flow involving a non-Newtonian fluid through a deformable parallel plate channel under the application of a flow rate crossing the inlet. The channel in its undeformed configuration has a height H and is bored in a PDMS block, which has been clamped rigidly such that the thickness of the solid wall that undergoes deformation is δ. We assume that the outer surface is excluded from the effects of deformation at the fluid-solid interface. The channel is assumed to extend infinitely in the $z-$direction such that the pressure gradient is strictly along the axis. A coordinate system is set up with the $x-$axis along the channel centre line and the $y-$axis perpendicular to it. In the undeformed configuration, the fluid is in the domain $x \in [0, L]$ and $y \in [0, H]$. We represent the deformation of the fluid-solid interface by $\mathcal{H}(x)$ calculated from the undeformed point at a distance H from the axis around the channel, and varies in the $x-$direction due to the varying amount of fluid pressure. Thus, the deformed channel height becomes $h = H + \mathcal{H}(x)$. We consider a neutrally buoyant rigid particle of radius a suspended in the fluid and does not interact with the channel walls or other particles.

2.1 Fluid

We consider an incompressible laminar flow of a Giesekus fluid having mobility parameter α, relaxation time λ, and viscosity η. We neglect the body forces and write the continuity

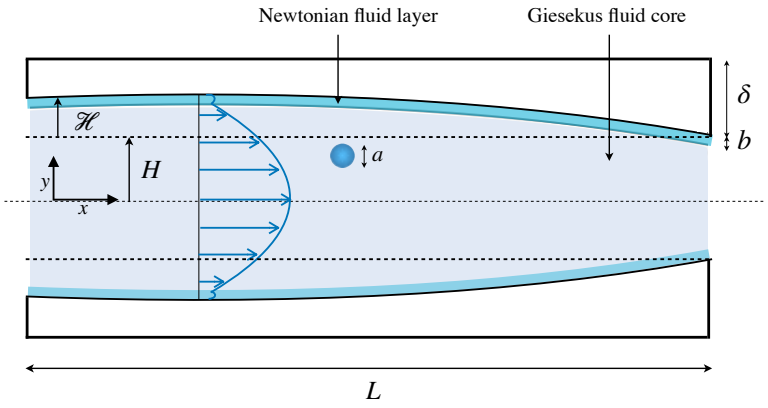

Figure 2.1: Schematic of the channel geometry shown in a deformed state with a neutrally buoyant particle. The inner core is comprised of the Giesekus fluid that is surrounded by a Newtonian fluid layer of thickness b.

and Stokes equation:

$$\nabla \cdot \boldsymbol{v} = 0, \tag{2.1}$$

$$\mathbf{0} = -\nabla P + \nabla \cdot \boldsymbol{\tau}, \tag{2.2}$$

where the velocity field $\boldsymbol{v} = \boldsymbol{v}(v_x, v_y, 0)$, the extra stress of the fluid and the hydrostatic pressure are represented by τ and P, respectively. The deformation at the interface shall give rise to weak velocity gradients in the $y-$direction but we neglect any such effects and assume $v_y = 0$. The following dimensionless variables are introduced for the quantities governing the flow: $y^* = y/H, v_x^* = v_x/V, x^* = x/L, P^* = PH/\eta V$, $\mathcal{H}^* = \mathcal{H}/H_s$, $\tau^* = \tau H/\eta V$ and Deborah number $De = \lambda V/H$ where H_s, V, P_s, and λ are the deformation length scale, characteristic velocity and pressure scale respectively. Eq. (2.1) can be non-dimensionalised using our scales:

$$\frac{\partial P^*}{\partial x^*} = \frac{L}{H}\frac{\partial \tau_{xy}^*}{\partial y^*} \tag{2.3a}$$

$$\frac{\partial P^*}{\partial y^*} = \frac{\partial \tau_{yy}^*}{\partial y^*} \tag{2.3b}$$

Since $\dfrac{\partial P^*}{\partial x^*}$ is a function of x^*, we can write Eq. (2.3)(a) as:

$$\tau^*_{xy} = \mathcal{G} y^*, \tag{2.4}$$

where $\mathcal{G} = \dfrac{H}{L}\dfrac{\partial P^*}{\partial x^*}$. We write the constitutive equation for a Giesekus fluid as:

$$\boldsymbol{\tau} + \lambda\left[\frac{\partial \boldsymbol{\tau}}{\partial t} + \boldsymbol{v}\cdot\nabla\boldsymbol{\tau}\right] - \lambda\left[\boldsymbol{\tau}\cdot(\nabla\boldsymbol{v}) + (\nabla\boldsymbol{v})^T\cdot\boldsymbol{\tau}\right] + \frac{\lambda\alpha}{\eta}\boldsymbol{\tau}\cdot\boldsymbol{\tau} = 2\eta\boldsymbol{D}, \tag{2.5}$$

where $\boldsymbol{D}$ is the deformation rate tensor. We reduce Eq. (2.5) into its dimensionless orthogonal components to arrive at:

$$\tau^*_{yy} + \alpha De\left(\tau^{*2}_{yy} + \tau^{*2}_{xy}\right) = 0 \tag{2.6a}$$

$$\tau^*_{xy} + \alpha De\tau^*_{xy}\left(\tau^*_{yy} + \tau^*_{xx}\right) - De\tau^*_{yy}\dot{\gamma}^* = \dot{\gamma}^* \tag{2.6b}$$

$$\tau^*_{xx} + \alpha De\left(\tau^{*2}_{xy} + \tau^{*2}_{xx}\right) - 2De\dot{\gamma}^*\tau^*_{xy} = 0 \tag{2.6c}$$

. From some algebraic manipulations using Eq. (2.6)(a),(b) and (c), we arrive at the expression of the shear rate :

$$\dot{\gamma}^* = \frac{1 + (2\alpha - 1)De\tau^*_{yy}}{(1 + De\tau^*_{yy})^2}\tau^*_{xy}, \tag{2.7}$$

We expand Eq. (2.6)(a) binomially to get an approximate solution of $\tau^*_{yy} \approx -\alpha De\tau^{*2}_{xy}$ [28]. We evaluate the axial velocity from Eq. (2.4) and Eq. (2.7) using $v^*_x = \int \dot{\gamma}^* dy^*$. We assume $\epsilon = H_s/H$ as the deformation parameter and the flow is subject to the no-slip boundary condition at the fluid-structure interface and a symmetric condition for velocity at the centreline which gives $v^*_x|_{h^*=1+\epsilon\mathcal{H}^*-b^*} = v^*_c$ and $\left.\dfrac{\partial v^*_x}{\partial y^*}\right|_{y^*=0} = 0$ respectively. This leads to $\tau_o = 0$ and we obtain the final expression for axial velocity:

$$v^*_x = -\frac{1}{2\alpha De^2\mathcal{G}}\Big(\Lambda(y^*) - \Lambda(1 + \epsilon\mathcal{H}^* - b^*)\Big) + v^*_c, \tag{2.8}$$

where,

$$\Lambda(y^*) = \frac{2(\alpha-1)}{1-\alpha De^2\mathcal{G}^2 y^{*2}} + (2\alpha-1)\ln\left[1-\alpha De^2\mathcal{G}^2 y^{*2}\right]$$

For the Newtonian fluid of viscosity μ, we can simply write

$$0 = -\frac{\partial P}{\partial x} + \mu\frac{\partial^2 u_n}{\partial y^2} \tag{2.9}$$

We denote the interface distance as $d^* = 1 + \epsilon\mathcal{H}^* - b^*$, where $b = b^* H_s$ is the thickness of the Newtonian layer. The two-fluid system is simultaneously solved taking the continuity of velocity and the shear stress at the fluid-fluid interface at $y^* = d^*$, that can be written as $v_c^* = v_x^*$ and $\frac{\mu\partial v_x^*}{\eta\partial y^*} = -y^*\left[2(\alpha-1)/(1-\alpha De^2\mathcal{G}^2y^{*2})^2 - (2\alpha-1)/(1-\alpha De^2\mathcal{G}^2y^{*2})\right]$ respectively, and we obtain:

$$v_c^* = \frac{\eta b^*\mathcal{G}}{2\mu}\left[-b^* + \frac{4(\alpha-1)d^*}{(1-\alpha De^2\mathcal{G}^2 d^{*2})^2} - \frac{2(2\alpha-1)d^*}{1-\alpha De^2\mathcal{G}^2 d^{*2}}\right]$$

Finally we obtain the velocity profile of the Newtonian fluid layer as:

$$\begin{aligned} u_n^* = \frac{\eta\mathcal{G}}{2\mu}y^{*2} - \frac{1}{b^*}\left[v_c^* + \frac{\eta\mathcal{G}b^*}{2\mu}(2+2\epsilon\mathcal{H}^*-b^*)\right]y^* - \frac{\eta\mathcal{G}}{2\mu}(1+\epsilon\mathcal{H}^*)^2 + \\ \frac{1+\epsilon\mathcal{H}^*}{b^*}\left[v_c^* + \frac{\eta\mathcal{G}b^*}{2\mu}(2+2\epsilon\mathcal{H}^*-b^*)\right] \end{aligned} \tag{2.10}$$

We define the non-dimensional volumtric flow rate per unit width as $Q^* = Q/HV = \int_0^{d^*} v_x^* dy^* + \int_{d^*}^{1+\epsilon\mathcal{H}(x)} u_n^* dy^*$ which is essentially constant for across the channel implying

$\frac{dQ^*}{dx^*} = 0$. We define $\phi = \mathcal{G}De\sqrt{\alpha}(1 + \epsilon\mathcal{H}^* - b^*)$ to obtain:

$$\begin{aligned} Q^* = -\frac{1}{\alpha De^2\mathcal{G}}\Bigg[\frac{3\alpha-2}{De\mathcal{G}\sqrt{\alpha}}\tanh^{-1}\phi - (2\alpha-1)(1+\epsilon\mathcal{H}^*-b^*) - \frac{(\alpha-1)(1+\epsilon\mathcal{H}^*-b^*)}{1-\phi^2}\Bigg] \\ +b^*\left[\frac{\eta\mathcal{G}}{2\mu}(1+2\epsilon\mathcal{H}^*-b^*) - \frac{1}{b^*}\left\{v_c^* + \frac{\eta\mathcal{G}b^*}{2\mu}(2+2\epsilon\mathcal{H}^*-b^*)\right\}(2+2\epsilon\mathcal{H}^*-b^*)\right] \\ -\frac{\eta b^*\mathcal{G}}{2\mu}(1+\epsilon\mathcal{H}^*)^2 + (1+\epsilon\mathcal{H}^*)\left[v_c^* + \frac{\eta\mathcal{G}b^*}{2\mu}(2+2\epsilon\mathcal{H}^*-b^*)\right]. \end{aligned} \tag{2.11}$$

2.2 Solid

The deformation of the interface as a consequence of fluid pressure is modelled using the Cauchy equation of motion and neglecting body forces,

$$\nabla \cdot \boldsymbol{\sigma} = \mathbf{0}, \tag{2.12}$$

where the deformation field $\boldsymbol{u} = \boldsymbol{u}(u_r, u_\theta, u_z)$ with $\boldsymbol{\sigma}$ representing the stress tensor which can be expressed as $\boldsymbol{\sigma} = G_1(\nabla \cdot \boldsymbol{u})\mathbf{I} + G_2[(\nabla\boldsymbol{u}) + (\nabla\boldsymbol{u})^T]$, where G_1 and G_2 are the Lamé parameters (with G_2, alternatively, referred to as the shear modulus). We consider the deformation to be constant in the $x-$direction. We write the various components of the stress tensor as:

$$\begin{aligned} \sigma_{xx} &= G_1\left(\frac{\partial u_x}{\partial x} + \frac{\partial u_y}{\partial y}\right) + 2G_2\frac{\partial u_x}{\partial x}, \\ \sigma_{yy} &= G_1\left(\frac{\partial u_x}{\partial x} + \frac{\partial u_y}{\partial y}\right) + 2G_2\frac{\partial u_y}{\partial y}), \\ \sigma_{xy} &= G_2\left(\frac{\partial u_x}{\partial y} + \frac{\partial u_x}{\partial y}\right). \end{aligned}$$

Non-dimensionalisation of Eq. (2.12) is done using the following scheme: $u_y^* = u_y/H_s, \kappa = \delta/H$. We then use the condition that deformation occurs only in the $y-$direction and $H \ll L$ which after appropriate substitution of Eq. (2.12) using the non-dimensionalised variables we get the reduced governing equation for the solid:

$$\frac{\partial^2 u_y^*}{\partial {y^*}^2} = 0. \tag{2.13}$$

We subject the solid to a no deformation condition at the outer boundary: ${u_y}^*|_{y^*=1+\kappa} = 0$ and impose traction balance at the inner boundary: $\sigma_{yy}|_{y^*=1+\epsilon\mathcal{H}(x)^*} = -P$. Since the deformation is same for both fluid and solid at the interface, we can write ${u_y}^*|_{y^*=1+\epsilon\mathcal{H}(x)^*} = \mathcal{H}(x)^*$. From the traction balance and using the stress relation for σ_{yy} we have:

$$\mathcal{H}^* = \frac{\kappa P^*}{1+\epsilon P^*}\cdot \tag{2.14}$$

Summarily, we have the two fluid system, where the inner core follows the Giesekus constitutive relation that governs the stress distribution as given in Eq. (2.5). The Newtonian fluid follows the Newton's law of viscosity where $\tau = \mu\dfrac{\partial u_n}{\partial y}$. Both the fluids are governed by Eq. (2.2). There is a shear stress continuity at the fluid-fluid interface and a normal stress continuity at the fluid-solid interface.

Lateral migration

Non-Newtonian fluids in shear flow experience normal stress differences [26], which are exactly zero for Newtonian fluids undergoing shear flow. The first and second normal stress differences are represented by $N_1 = \tau_{yy} - \tau_{xx}$ and $N_2 = \tau_{zz} - \tau_{yy}$ respectively. For most polymeric suspensions in shear flows, N_1 is usually positive, and N_2 is negative [29]. These extra stresses play an important role in many rheological phenomena [30], and motion can be imparted as tension builds along the streamlines. Suspended particles have been demonstrated to show migration in pressure-driven flows by the influence of such stresses giving rise to elastic forces [17]. The analysis was carried out for a rigid rectangular channel, and we extend it to a parallel plate channel with deformable walls. We represent N_1 and N_2 as the difference of stress components, which is a more generalised representation than an empirical approximation through power law relation with the shear rate as was considered in [17] and we also neglect the contribution of N_2 [31]. The particle is in equilibrium under the action of elastic forces that develop due to the variation in N_1 and drag forces that arise due to fluid viscosity. We perform a balance between these forces [17] in the $y-$direction to determine the migration velocity $v_\perp$ in that direction. The elastic and drag forces can be represented as $F_e = \varphi a^3 \nabla_y N_1$ and $F_d = -6\pi\eta a v_\perp$ respectively, where φ is a positive constant.

We formulate a particle distribution function (PDF) to visualise the migration of the particles through their probable distribution across the channel. It must be noted that the Newtonian fluid layer does not allow the development of normal stress differences in it, there

naturally eliminating the possibility of any migration of particles. The effective domain of migration thus reduces to $H + \mathcal{H} - b$ from the centreline. Let Γ and $\boldsymbol{J} = \Gamma v_\perp \hat{\boldsymbol{j}}$ represent the probability density and the probability current vector respectively, such that the probability of the particle at a given axial position x_o is $\Gamma(x_o, y)$. The probability density function satisfies the equation $\frac{\partial \Gamma}{\partial t} + \nabla \cdot \boldsymbol{J} = 0$ which can be reduced to $\nabla \cdot (\Gamma \boldsymbol{v}) = 0$ for steady state. We solve this to obtain:

$$\Gamma = \Gamma_o \frac{v_{\perp o}}{v_\perp}. \tag{3.1}$$

To obtain the probability function at a particular y, we calculate the total probability till that point and get:

$$\Gamma_y = \frac{\Gamma}{\int_0^y \Gamma dy}. \tag{3.2}$$

where Γ_o and $v_{\perp o}$ are the values of Γ and $v_\perp$ at (x_o, y_o). This is evaluated along with a convolution of Γ with a Gaussian curve to represent the final normal distribution of particles along the channel height at a particular axial distance from the inlet.

$$\psi = \frac{1}{\sqrt{2\pi} S} \int_0^y \Gamma_y (y - w) \exp\left[-\frac{w}{2S^2}\right] dw. \tag{3.3}$$

where S is the standard deviation of the distribution. An approximate analytical solution can also be determined for flows in the limit $\alpha De \tau^*_{xy} \ll 1$ [28]. In such limits, we can approximate $\nabla_y N_1 \approx 2\alpha\eta De^2 \mathcal{G}^2 y / H^2 \lambda$, thus allowing us to obtain a simplified form after balancing the forces:

$$v_\perp = -\varphi \frac{a^2 \alpha De^2 \mathcal{G}^2}{3\pi\lambda H^2} y. \tag{3.4}$$

The negative sign shows the inward nature of this migration towards the channel centreline and follows an approximate linear variation similar to Naillon et al. [32] and Romeo et al. [2]. As the particle flows away from the inlet and starts to migrate towards the centre, it reaches a particular y at different locations depending on several parameters. Let a particle initially near the wall at a height $H - a$ at the inlet, eventually attains a

height of y_o at a distance x_o from the start. From Eq. (3.4) we can evaluate this convergence length as the migration can be represented through $dy/dt = v_\perp$. Expressing Eq. (3.4) as $v_\perp = \mathcal{C}y$, we can write the lateral trajectory as:

$$\int_{H-a}^{y_o} \frac{dy}{y} = \int_0^{\Delta t} \mathcal{C} dt \tag{3.5}$$

where $\Delta t = \dfrac{x_o}{Q/\pi R^2}$ is the average time required to the particle to travel a horizontal distance of x_o. A simplified analytical expression can be written as:

$$x_o = -\frac{3\pi H^3}{\varphi a^2 \alpha De \mathcal{G}^2} \ln\left(\frac{y_o}{H-a}\right). \tag{3.6}$$

Solution strategy

We formulate a numerical scheme for the simultaneous solution of Eq. (2.14) and $dQ^*/dx^* = 0$. We use the approximation that $b^* << 1$ which allows us to neglect the contribution from the Newtonian part and we re-write the equation of flow rate as derived in Eq. (2.11):

$$Q^* = -\frac{1}{\alpha De^2 \mathcal{G}}\Big[\frac{3\alpha-2}{De\mathcal{G}\sqrt{\alpha}}\tanh^{-1}\phi - (2\alpha-1)(1+\epsilon\mathcal{H}^*) - \frac{(\alpha-1)(1+\epsilon\mathcal{H}^*)}{1-\phi^2}\Big]. \tag{4.1}$$

Differentiating Eq. (4.2) w.r.t x^*, we obtain the following relation:

$$\begin{aligned} 2\Lambda_1 Q^*\mathcal{G}\left[(1-\phi^2)\frac{d\mathcal{G}}{dx^*} - \mathcal{G}\phi\frac{d\phi}{dx^*}\right] - (\Lambda_2+\Lambda_3-\Lambda_2\phi^2)\left[\mathcal{G}\epsilon\frac{d\mathcal{H}^*}{dx^*} + (1+\epsilon\mathcal{H}^*)\frac{d\mathcal{G}}{dx^*}\right] \\ + \frac{d\phi}{dx^*}\left[2\Lambda_4\phi\ln\left(\frac{1+\phi}{1-\phi}\right) - 2\Lambda_4 + 2\Lambda_2\phi\mathcal{G}(1+\epsilon\mathcal{H}^*)\right] = 0 \end{aligned} \tag{4.2}$$

where $\Lambda_1 = -De^3\alpha^{3/2},\ \lambda_2 = (1-2\alpha)De\sqrt{\alpha},\ \Lambda_3 = (1-\alpha)De\sqrt{\alpha}$ and $\Lambda_4 = 3/2\alpha - 1$. This allows us to formulate our Newton-Raphson multivariate scheme. For the set of generally non-linear equations in $x_k, k = 1, 2..., n,\ F_j(x_k) = 0, j = 1, 2..., n,\ k = 1, 2..., n$. We obtain the solutions of the linearly independent equations through iterations as:

$$X^{m+1} = X^m + (J^m)^{-1}R^m, \quad \text{till} \quad ||\mathrm{R}|| < \text{tolerance} \tag{4.3}$$

where m is the iteration index, and

$$X_k = x_k, \quad \mathrm{k} = 1, 2...\mathrm{n}$$

$$R_k = F_k, \quad \mathrm{k} = 1, 2...\mathrm{n}$$

$$J_{k,j} = \frac{\partial F_k}{\partial x_j}, \quad \mathrm{k} = 1, 2...\mathrm{n}, \ \mathrm{j} = 1, 2...\mathrm{n}$$

For the set of equation of our system:

$$\phi_i = x_i, \quad \mathrm{i} = 1, 2...\mathrm{n}$$

$$\mathcal{G}_i = x_{n+i}, \quad \mathrm{i} = 1, 2...\mathrm{n}$$

$$\mathcal{H}_i^* = x_{2n+i}, \quad \mathrm{i} = 1, 2...\mathrm{n}$$

$$P_i^* = x_{3n+i}, \quad \mathrm{i} = 1, 2...\mathrm{n}$$

Thus we get,

$$R_i = \mathcal{G}_i De\sqrt{\alpha}(1 + \epsilon\mathcal{H}_i^*) - b^* - \phi_i, \quad \mathrm{i} = 1, 2...\mathrm{n}$$

$$R_{n+i} = \begin{cases} \mathcal{G}_i - H/L\left(P_{i+1}^* - P_i^*\right)/(x_{i+1}^* - x_i^*), & \mathrm{i} = 1 \\ \mathcal{G}_i - H/L\left(P_{i+1}^* - P_{i-1}^*\right)/2(x_{i+1}^* - x_i^*), & \mathrm{i} = 2...\mathrm{n} - 1 \\ \mathcal{G}_i - H/L\left(P_i^* - P_{i-1}^*\right)/(x_i^* - x_{i-1}^*), & \mathrm{i} = \mathrm{n} \end{cases}$$

$$R_{2n+i} = (1 + \epsilon P_i^*)\mathcal{H}_i^* - \kappa P_i^*, \quad \mathrm{i} = 1, 2...\mathrm{n}$$

$$R_{3n+i} = 2\Lambda_1 Q^* \mathcal{G}\left[(1-\phi^2)\frac{d\mathcal{G}}{dx^*} - \mathcal{G}\phi\frac{d\phi}{dx^*}\right] - (\Lambda_2 + \Lambda_3 - \Lambda_2\phi^2)\left[\mathcal{G}\epsilon\frac{d\mathcal{H}^*}{dx^*} + (1+\epsilon\mathcal{H}^*)\frac{d\mathcal{G}}{dx^*}\right] + \frac{d\phi}{dx^*}\left[2\Lambda_4\phi\ln\left(\frac{1+\phi}{1-\phi}\right) - 2\Lambda_4 + 2\Lambda_2\phi\mathcal{G}(1+\epsilon\mathcal{H}^*)\right], \quad \mathrm{i} = 1, 2...\mathrm{n}$$

Through this we are able to obtain the values of $\phi^*(x^*), \mathcal{G}(x^*)$, $\mathcal{H}^*(x^*)$ and $P^*(x^*)$. Subsequently, we arrive at the stress components in the fluid through the relations:

$$\tau^*_{xy} = \mathcal{G} y^* \tag{4.7a}$$

$$\tau^*_{yy} = \frac{-1 + \sqrt{1 - 4\alpha^2 De^2 \tau^{*2}_{xy}}}{2\alpha De} \tag{4.7b}$$

$$\tau^*_{xx} = \dot{\gamma} \frac{1 + De\tau^*_{yy}}{\alpha De \tau^*_{xy}} - \frac{1 + \alpha De \tau^*_{yy}}{\alpha De} \tag{4.7c}$$

This allows us to obtain the numerical solution of v_x through Eq. (2.8). We also have the numerical solution of $v_\perp$ through the balance of forces as described to give:

$$v_\perp = -\varphi \frac{a^2}{6\pi\eta} \frac{\partial N_1}{\partial y} \tag{4.8}$$

The neutrally buoyant particle, under equilibrium of forces, acquires a velocity $\boldsymbol{v} = v_x \hat{\boldsymbol{i}} + v_\perp \hat{\boldsymbol{j}}$. The velocity distribution is symmetrical about the centreline and the particle migrates laterally in the region $y \in [0, H + \mathcal{H} - b]$ in the upper half.

Results and discussion

Following the mathematical description of the flow, the neutrally buoyant particle moves forward along the channel combined with a tendency to migrate towards the centreline. The intersection point on the plane $\mathbb{P}$, at a distance y_o from the axis, is denoted by the distance x_o from the inlet, which depends on various factors as seen from Eq. (3.6). The channel geometry and the pressure gradient play an important part in governing the flow and both are heavily influenced by the channel deformability according to Eq. (2.14). A rigid walled channel can be approximated of having high Young's modulus E such that the pressure gradient is uniform. A non-uniform pressure gradient is an essential aspect of a flow through a deformable channel and is captured by $\mathcal{G}$. The neutrally buoyant particle of radius $a = 0.5\mu$m, unless stated otherwise, is assumed to be released at a distance $H - a$ at the inlet, perpendicular to the centreline, which meets $\mathbb{P}$ after traversing a distance x_o in the axial direction. The theoretical convergence length expressed through Eq. (3.6) has been shown in Fig. 5.1 for different plane heights y_o. Since our analysis pertains to a rectangular channel and the determination of φ is usually done experimentally, we proceed with a hypothetical value of φ. Without loss of generality, the value of φ is assumed to demonstrate the correspondence of our results with the observation made in D'Avino et al. [1] for a circular channel. It is observed in Fig. 5.1, which shows the effect of wall deformability and also presents convergence length variation for rigid channels. The convergence length clearly increases with an increase in wall deformability as represented by a smaller value of E and taking Poisson's ratio of 0.48. On a qualitative front, the deformable channel height increases in response to the fluid

pressure, and the tendency of migration is attenuated, leading the particle to travel farther before meeting the centreline. From Eq. (3.6), it is evident that x_o varies inversely with the pressure gradient, and for a fixed volumetric flow rate Q, $\mathcal{G}$ decreases with an increase in flow cross-sectional area, which happens for a softer wall. The Deborah number can be related to the flow rate as $De = \lambda Q/H^2$. As De increases, convergence length decreases for a particular value of E, indicating faster migration at higher flow rates. We see a shift in the overall data by an offset in the presence of the Newtonian fluid layer in Fig. 5.1(b) that suggests smaller convergence length which in turn points at the possibility of faster migration due to a constricted space where normal stress differences exist. Such a trend has also been observed in Leshansky et al. [17] where the effect of flow rate on particle migration was studied.

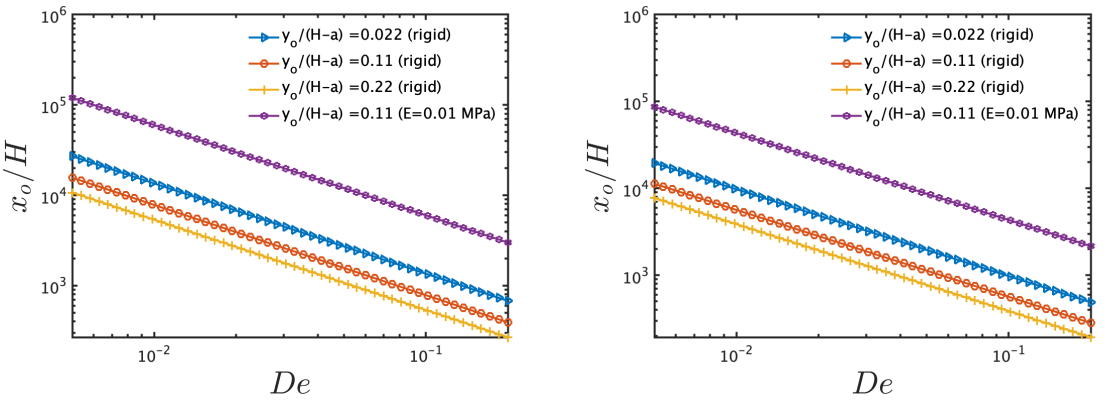

(a) Simplified flow

(b) Flow with Fåhræus-Lindqvist effect

Figure 5.1: Ratio of convergence length to undeformed half channel height variation with Deborah number for different release positions of the particle at inlet. The distinct effect of deformable wall is visible along with comparison with D'Avino et al. [1]. We see the effect of the presence of a Newtonian fluid layer in (b) as compared to a single fluid system in (a).

The trajectory of the particles are governed through the relation $dy/dx = v_\perp/v_x$. The particles migrate towards the axis as they flow, thereby leading to a case when they might meet the axis prior to reaching the end of the channel. It might also happen, that their paths

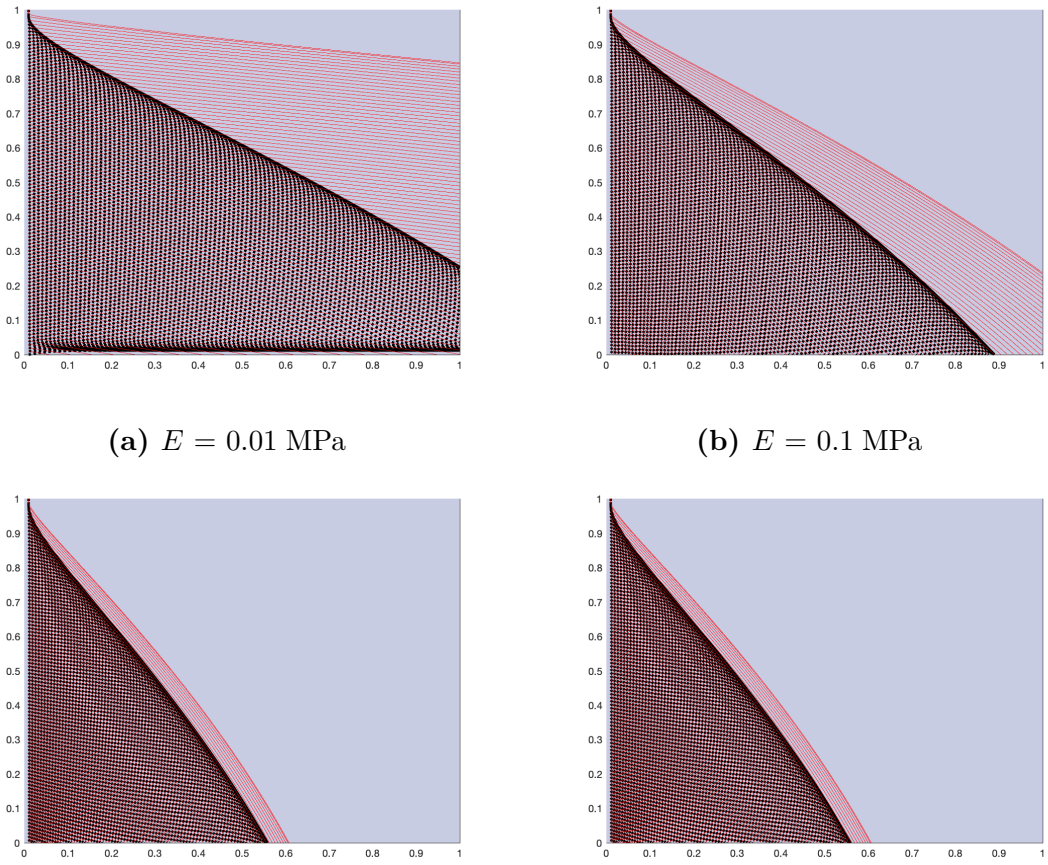

(a) $E = 0.01$ MPa

(b) $E = 0.1$ MPa

(c) $E = 100$ MPa

(d) $E = 10000$ MPa

Figure 5.2: The trajectory of particles for different wall softness, with $De = 0.5$ shown in the $xy-$plane. Black plot denotes the effect of Fåhræus Lindqvist effect in contrast to the original flow shown in red.

overshoot the channel dimensions and they meet the outlet at a distance perpendicular to the axis. We investigate these situations in Fig. 5.2 where the effect of wall stiffness on the trajectories. We observe that the particles have the tendency to overshoot for softer channels for unchanged flow parameters. Rapid convergence is observed for rigid channels which was previously demonstrated in Fig. 5.1. We have simultaneously shown the effect of the two-fluid system in black which suggests the occurrence of faster convergence in the non-

Newtonian core region. it is important to notice that the presence of the Newtonian layer is more significant in softer walls than in stiffer walls. The higher degree of deformation in softer walls is lesser, leads to a higher variation in cross-section area, that is more significant in the former.

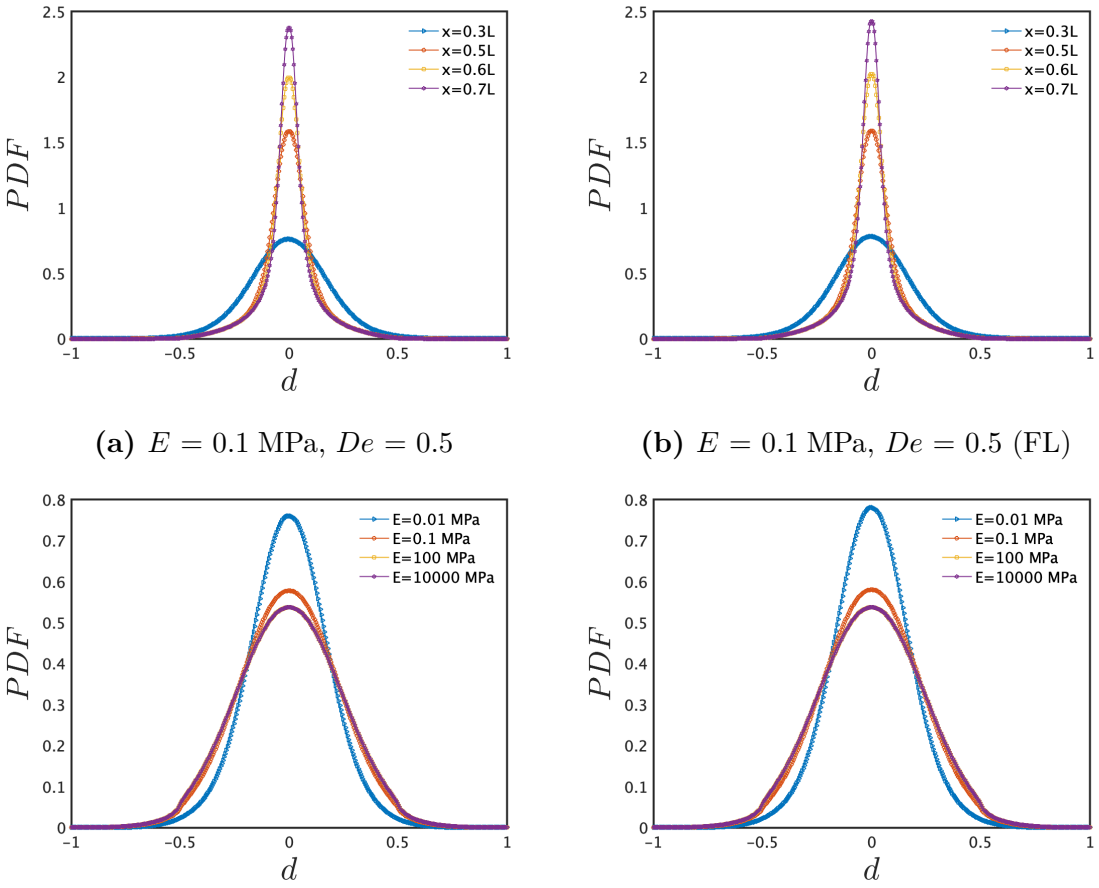

(a) $E = 0.1$ MPa, $De = 0.5$

(b) $E = 0.1$ MPa, $De = 0.5$ (FL)

(c) $x = 0.3$ L, $De = 0.5$

(d) $x = 0.3$ L, $De = 0.5$ (FL)

Figure 5.3: Particle distribution functions across the channel cross-section is shown for different scenarios. FL denotes the presence of Fåhræus-Lindqvist effect. Other flow and geometric parameters (λ,η,α,L,H,a) remain constant in each panel.

The particle distribution function is shown in Fig. 5.3 where the distributions have standard deviations depending on the uncertainty in the measurement of particle distance

depending on the deformed channel height at that distance from the inlet. Fig. 5.3(a) shows the effect of distance from the inlet on the particle distribution, demonstrating higher migration rates at farther positions from the inlet where the channel gradually gets narrower as pressure falls along the flow length. This gradual narrowing of the channel gives rise to a passive movement of the particles towards the centreline by constricting their flow. In Fig. 5.3(b) we observe that the distribution becomes nominally higher by $\sim 2\%$ compared to Fig. 5.3(a) upon modelling using the layer of Newtonian fluid. It again highlights the increased migration tendency owing to the Fåhræus-Lindqvist effect. The maximum change is observed at $x = 0.7L$ that suggests that cross-section changes more rapidly at the farther ends as compared to the entry zone. A stiffer channel has an approximate uniform cross-sectional area that reduces the tendency of migration compared to a tapered channel. The trend is otherwise followed as migration becomes faster at a point farther away from the inlet, as observed in Naillon et al. [32]. It becomes evident regarding the role of non-linear pressure gradient as well as effective migration region on migration tendency where both of the factors lead to its dominance in Fig. 5.3(a) over (b). The effect of wall stiffness is demonstrated in Fig. 5.3(c) where a higher deformation occurring in softer walls with lower values of E contributes to higher pressure gradients and a gradually narrowing flow cross-section area that enhances the migration in such scenarios. It is interesting to note that in Fig. 5.1, we had observed higher convergence length for softer walls, which might indicate at lower migration tendencies, but as the channel gradually narrows down in such scenarios, the axial velocity increases, thereby allowing the particle to converge at a farther point although the migration tendency being higher. Once again, a maximum increase of $\sim 2.6\%$ in the distribution heights has been observed in Fig. 5.3(d) owing to the Fåhræus-Lindqvist effect. This increase is highest for the softest channel as the degree of deformation is maximum, which in turn leads to a higher degree of taper and changes in cross-section occurs rapidly. The shrinking of the core region of migration affects the distribution to a larger extent.

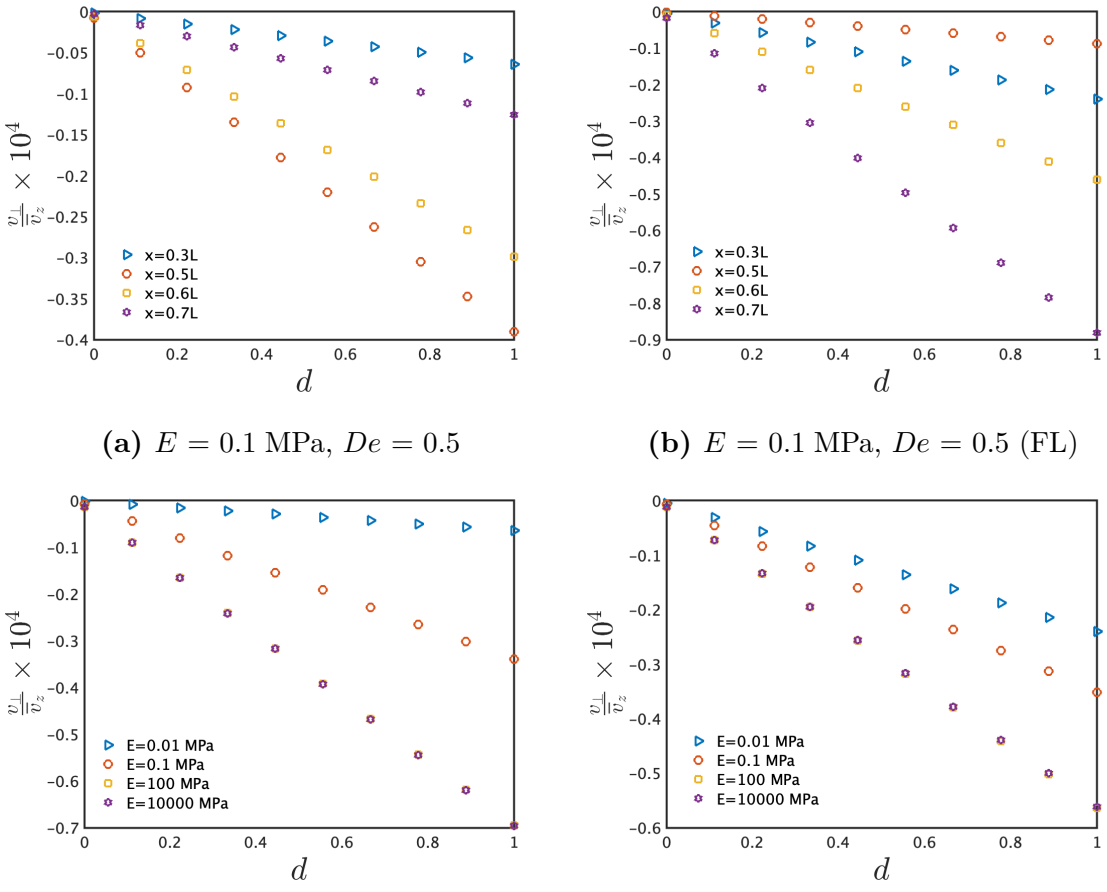

(a) $E = 0.1$ MPa, $De = 0.5$

(b) $E = 0.1$ MPa, $De = 0.5$ (FL)

(c) $x = 0.3$ L, $De = 0.5$

(d) $x = 0.3$ L, $De = 0.5$ (FL)

Figure 5.4: Migration velocity variation across the channel cross-section, expressed as a ratio with the average axial velocity is shown. The trend in can be contrasted with the observations made in [2]. FL denotes the presence of Fåhræus-Lindqvist effect.

The relative magnitudes of $v_\perp$ and v_x is a critical factor governing the trajectory of the particle. We have seen that flows with higher migration tendencies can have longer convergence lengths depending on the axial flow velocity strength. We represent the ratio of $v_\perp$ and the mean axial velocity $\overline{v}_x$ in Fig. 5.4 across the channel height where $d = y/h$. The approximate linear variation of $v_\perp$ can be related to the prediction made through Eq. (3.4). Fig. 5.4(a) shows the increase in migration velocity as we move away from the centreline

since $\overline{v}_z$ is constant for a particular cross-section. The ratio $v_\perp/\overline{v}_x$ does not seem to follow a particular order according to the positions relative to the channel inlet in Fig. 5.4(a). Such an anomaly in trend is observed in Fig. 5.4(b) concerning the Fåhræus Lindqvist effect. This deviation in Fig. 5.4(a) can be attributed to the fact that v_x increases along the channel length for a deformable channel rather than being constant for a rigid channel considered in [2]. Both $v_\perp$ and v_z depend on geometry and their relative magnitudes cannot be said to follow the trend observed in Romeo et al. [2] and Fig. 5.4(d) significantly deviates from it. The presence of an additional layer of fluid alters the sequence of $v_\perp/\overline{v}_x$ as observed in Fig. 5.4(b) where the relative interplay between the two velocities cannot be said affirmatively predicted. v_z is heavily dependent on the cross-sectional area at a location whereas $v_\perp$ is significantly affected by the rate of change of cross-section owing to the deformation profile of the wall. The area of cross-section varies with $1 + \epsilon\mathcal{H}^* - b^*$, where $b^* = 0$ in absence of Faåhræus-Lindqvist effect whereas the rate of deformation varies as $d\mathcal{H}^*/dx^*$ and their ratio is a surjective function. This non-monotonic variation is a profound effect of channel deformation leading to non-linear pressure gradient, and a tapering cross-section. Fig. 5.4(c) demonstrates a similar trend where at a particular cross-section, $|v_\perp/\overline{v}_x|$ increases with an increase in stiffness for a fixed d. This suggests that v_x remains constant and $|v_\perp|$ increases along the channel for a fixed perpendicular distance from the centreline. As E approaches higher values, no significant change in velocity is observed in response to change in E for 100 MPa and 10 GPa. We notice that in Fig. 5.4(d), significant deviations take place from Fig. 5.4(c) for softer channels, and the ratio increases, pointing at the increased migration tendency that corroborates with Fig. 5.1(d).

We also show the particle distribution in presence of the Fåhræus-Lindqvist effect for different sphere radius of the suspended particles and also for different shear-thinning behaviour, which is attributed to the mobility parameter of a Giesekus fluid. It was observed by Leshansky et al. [17] that the PDF distribution is narrower for larger particles which is in agreement with Fig. 5.5(a) and indicates higher migration tendency according

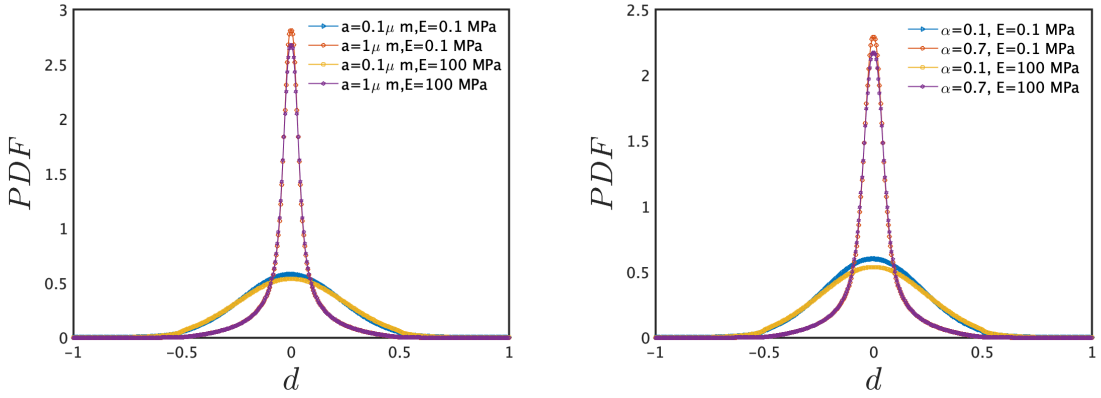

(a) $De = 0.5$, $x = 0.3$ L **(b)** $De = 0.5$, $x = 0.3$ L

Figure 5.5: Particle distribution functions across the channel cross-section is shown for different scenarios. Other flow and geometric parameters (λ,η,L,H) remain constant in each panel.

to Eq. (3.4). It also shows the effect of wall deformability whose effect on the distribution is highly eclipsed by the effect of particle size. An increase in α increases the shear-thinning behaviour as we see a rise in the lateral migration in Fig. 5.5(b). It was observed that particles have lower tendency to migrate for weaker shear-thinning fluids [33, 34] which is in agreement with our data. The effect of shear-thinning behaviour is more pronounced on particle distribution than the wall deformability which is seen as well from Fig. 5.5(b).

The addition of a Newtonian layer of thickness b decreases the effective region of migration to $H + \mathcal{H} - b$ for a channel of undeformed height H and deformation profile $\mathcal{H}$. Considering another scenario for a channel of undeformed height $H - b$, that does not have a Newtonian fluid layer, the deformation profile $\mathcal{H}_1$ will not be $\mathcal{H}$ anymore. Fig. 5.6 shown how the deformation profiles are not shifted by an offset for different channel heights that satisfies the above explanation. This shows how the development of a Newtonian layer cannot be mimicked otherwise unless we introduce changes in the properties of the linearly-isotropic elastic solid for the channel of height $H - b$ such that $\mathcal{H}_1 = \mathcal{H}$ for the same flow conditions. Such evolution of the fluid-fluid interface has been studied in [35]

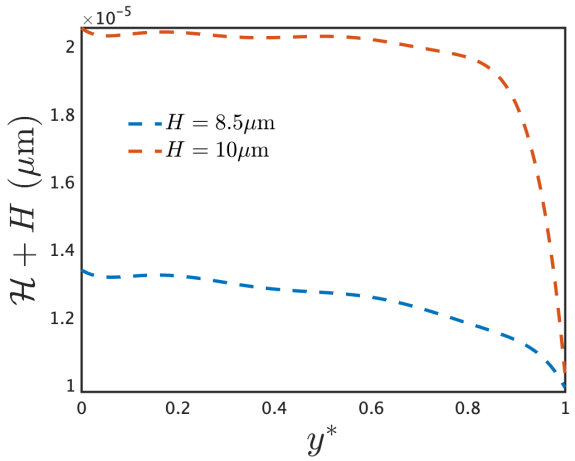

Figure 5.6: The difference between the particle distribution functions across the channel cross-section in the presence and absence of the Fåhræus-Lindqvist effect for different axial location with $E = 0.1$ MPa, $De = 0.5$.

that highlights the non-conformal shape of the interface with the solid boundary. The variations in the interface is entirely controlled by the movement of the channel wall and viscous forces from the two fluids acting on the interface. There has been studies aimed to address the competition between wall-induced migration and shear-induced diffusion [36]. The thickness of the particle depleted layer was found to be dependent on the capillary number. The decrease in the thickness increases the flow resistance of suspended particles, which is contrasting to the observed effects of addition of polymers in blood flow. Neglecting the existence of this layer would lead to significant deviations in predicting electroosmotic transport of such fluids [37]. Flow-induced segregation phenomena in multicomponent suspensions such as blood have been studied in [38] where migration and volume exclusion near the wall are the key features of the model that captures this particle-free layer formation that is Newtonian in nature. Such depletion models that couples the distribution of haematocrit, shear rate and non-Newtonian viscosity to account for the migration and aggregation of RBCs have been shown in [39]. Viscosities tends to the plasma viscosity as the haematocrit tends to zero in the depletion layer, falling below

1% of the total count.

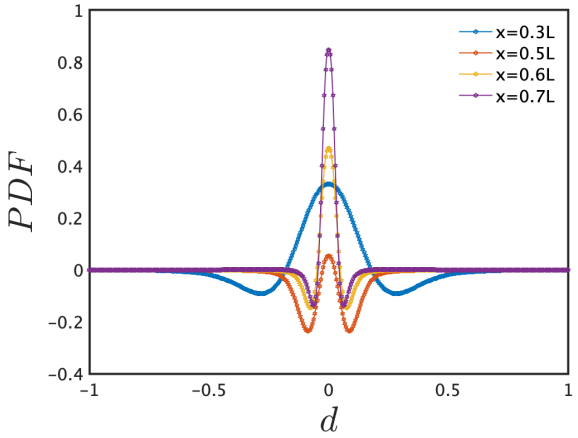

Figure 5.7: The difference between the particle distribution functions across the channel cross-section in presence and absence of the Fåhræus-Lindqvist effect for different axial location with $E = 0.1$ MPa, $De = 0.5$.

A very important demonstration of the Fåhræus-Lindqvist effect that concludes our study is the difference in the probability distribution function for the cases where the Newtonian fluid layer is absent (case 1) and present (case 2) as demonstrated in Fig. 5.7. It gives an indispensable insight on the stratification of migration velocities across the cross-section. It is quite interesting to notice that the migration for case 1 exceeds that of case 2 only within a region that changes according to location of the region from the channel inlet. We observe that this reversal distance b_0, measured from the centreline, decreases along the channel length. This can be interpreted in lines of an evolving Newtonian fluid layer, wherein the complete development of the layer will introduce a change in the migration characteristics, where it will be enhanced or slowed down depending on the distance b_0. The influence of various parameters on lateral migration has been studied, including the deformability, distance from the inlet, sphere radius and mobility parameter. We finally look into an important physiological parameter, Young's modulus of the solid which has a profound influence in imparting elastic character to this visco-elastic phenomenon. The

softness of the solid is related to it's deformability and we have seen how increasing Young's modulus E leads us to the approximate definition of a rigid solid and $v_\perp$ in such a case corresponds to the analysis done in [17] for a rigid rectangular channel.

The contribution of the deformability and the Fåhræus-Lindqvist effect on particle migration using a non-Newtonian fluid is largely indispensable and goes a long way to control the flow in numerous ways, including introducing a non-linear pressure gradient to a variation in axial velocity along the channel length. The migration velocity is seen to follow an approximately linear relation with distance from the axis and competes with the axial counterpart in many cases, often leading to direct or inverse relations. The formation of a particle free layer in the periphery is an important biomimetic model that alters the migration characteristics of particles. The solution has been obtained using equilibrium of forces using constant viscosity for each fluid instead of solving for the particle flow field that arises from a spatially varying viscosity in the Quemada model [39, 40].

Conclusion

We study the effect of deformable walls on particle migration in a Giesekus fluid, undergoing pressure-driven flow through an initially uniform parallel plate channel. We incorporate an additional physics arising from the Fåhræus-Lindqvist effect, leading to the development of a thin layer of Newtonian fluid that is hallmarked by the absence of normal stress differences. This leads to the absence of migratory behaviour in the thin annular region, leading to an effective rise in the lateral movement of the particles in the core, comprised of the non-Newtonian fluid. A numerical solution of the flow and the deformed geometry has been obtained. Such deformability ensures an array of contingent parameters that alter the flow in ways not dependent on the fluid properties. The suspended spheres experience forces of elastic nature due to the normal stress differences that were developed in shearing as well forces arising from viscosity. Migration becomes faster as the walls tend to deform, allowing for additional migration tendencies in a Newtonian fluid, devoid of elastic forces. This hints at novel methods of particle control in flows by altering channel geometry along with fluid properties. The wide variety of particle distributions for an array of solid and fluid properties attest to numerous tuning parameters to control migration and opens up the possibility of designing micro-channel flows of desired parameters.

This phenomenon can be extended to Newtonian fluids, where the inertial forces can be complemented with the motion resulting from deformation. The effect of particle radius as the velocity scales with the second power of a could lead to efficient particle sorting by controlling the channel sectional area at the various points. Deformed channels can

also be used to induce a tendency to migrate away from the axis as in the case of special fluids with negative first normal stress difference [18]. This study assumes that the interface between Newtonian and Giesekus is conformal with the solid-fluid interface. This major simplification is a limitation of this study. It must be noted carefully that a configuration with the Newtonian layer thickness b for a channel of undeformed height H does not yield similar migration characteristics with another channel of undeformed height $H - b$ and no Newtonian layer formation. This study can be extended to a more realistic model, where the shape of the fluid-fluid interface is itself a solution of the stress and velocity continuity relation that can be solved using iterative schemes. These findings are presumed to be of importance in understanding migration of particles in complex fluids, including biological fluids, that occur in confined microfluidic framework.

Bibliography

[1] G. D'Avino, G. Romeo, M. M. Villone, F. Greco, P. A. Netti, and P. L. Maffettone, "Single line particle focusing induced by viscoelasticity of the suspending liquid: theory, experiments and simulations to design a micropipe flow-focuser," *Lab on a Chip*, vol. 12, no. 9, pp. 1638–1645, 2012.

[2] G. Romeo, G. D'Avino, F. Greco, P. A. Netti, and P. L. Maffettone, "Viscoelastic flow-focusing in microchannels: scaling properties of the particle radial distributions," *Lab on a Chip*, vol. 13, no. 14, pp. 2802–2807, 2013.

[3] R. Fåhraeus, "The suspension stability of the blood," *Physiological Reviews*, vol. 9, no. 2, pp. 241–274, 1929.

[4] R. Fahraeus and T. Lindqvist, "The viscosity of the blood in narrow capillary tubes," *American Journal of Physiology-Legacy Content*, vol. 96, no. 3, pp. 562–568, 1931.

[5] R. Chebbi, "Dynamics of blood flow: modeling of the fåhræus–lindqvist effect," *Journal of biological physics*, vol. 41, no. 3, pp. 313–326, 2015.

[6] P. Bagchi, "Mesoscale simulation of blood flow in small vessels," *Biophysical journal*, vol. 92, no. 6, pp. 1858–1877, 2007.

[7] S. K. Doddi and P. Bagchi, "Three-dimensional computational modeling of multiple deformable cells flowing in microvessels," *Physical Review E*, vol. 79, no. 4, p. 046318, 2009.

[8] J. Y. Kim, S. W. Ahn, S. S. Lee, and J. M. Kim, "Lateral migration and focusing of colloidal particles and dna molecules under viscoelastic flow," *Lab on a Chip*, vol. 12, no. 16, pp. 2807–2814, 2012.

[9] G. Segré, "Radial Particle Displacements in Poiseuille Flow of Suspensions," , vol. 189, pp. 209–210, Jan. 1961.

[10] B. Ho and L. Leal, "Inertial migration of rigid spheres in two-dimensional unidirectional flows," *Journal of fluid mechanics*, vol. 65, no. 2, pp. 365–400, 1974.

[11] G. S. Blair, "An equation for the flow of blood, plasma and serum through glass capillaries," *Nature*, vol. 183, no. 4661, pp. 613–614, 1959.

[12] K. Kang, S. S. Lee, K. Hyun, S. J. Lee, and J. M. Kim, "Dna-based highly tunable particle focuser," *Nature communications*, vol. 4, no. 1, pp. 1–8, 2013.

[13] M. Brust, C. Schaefer, R. Doerr, L. Pan, M. Garcia, P. E. Arratia, and C. Wagner, "Rheology of human blood plasma: Viscoelastic versus newtonian behavior," *Phys. Rev. Lett.*, vol. 110, p. 078305, Feb 2013.

[14] W.-D. Shi, J. Wang, S. You, and W.-C. Yan, "Numerical simulation of particle focusing dynamics of dna-laden fluids in a microtube," *Chemical Engineering Science*, vol. 209, p. 115213, 2019.

[15] X. Hu, J. Lin, D. Chen, and X. Ku, "Influence of non-newtonian power law rheology on inertial migration of particles in channel flow," *Biomicrofluidics*, vol. 14, no. 1, p. 014105, 2020.

[16] R. V. Maitri, S. De, S. P. Koesen, H. M. Wyss, J. van der Schaaf, J. A. M. Kuipers, J. T. Padding, and E. A. J. F. Peters, "Effect of microchannel structure and fluid properties on non-inertial particle migration," *Soft Matter*, vol. 15, pp. 2648–2656, 2019.

[17] A. M. Leshansky, A. Bransky, N. Korin, and U. Dinnar, "Tunable nonlinear viscoelastic "focusing" in a microfluidic device," *Physical review letters*, vol. 98, no. 23, p. 234501, 2007.

[18] S. H. Yang, D. J. Lee, J. R. Youn, and Y. S. Song, "Double-line particle focusing induced by negative normal stress difference in a microfluidic channel," *Microfluidics and Nanofluidics*, vol. 23, no. 2, p. 21, 2019.

[19] D. Li, X. Lu, and X. Xuan, "Viscoelastic separation of particles by size in straight rectangular microchannels: A parametric study for a refined understanding," *Analytical Chemistry*, vol. 88, no. 24, pp. 12303–12309, 2016.

[20] K. W. Seo, Y. J. Kang, and S. J. Lee, "Lateral migration and focusing of microspheres in a microchannel flow of viscoelastic fluids," *Physics of Fluids*, vol. 26, no. 6, p. 063301, 2014.

[21] A. H. Raffiee, A. M. Ardekani, and S. Dabiri, "Numerical investigation of elasto-inertial particle focusing patterns in viscoelastic microfluidic devices," *Journal of Non-Newtonian Fluid Mechanics*, vol. 272, p. 104166, 2019.

[22] H. Lim, J. Nam, and S. Shin, "Lateral migration of particles suspended in viscoelastic fluids in a microchannel flow," *Microfluidics and nanofluidics*, vol. 17, no. 4, pp. 683–692, 2014.

[23] D. Alghalibi, M. E. Rosti, and L. Brandt, "Inertial migration of a deformable particle in pipe flow," *Phys. Rev. Fluids*, vol. 4, p. 104201, Oct 2019.

[24] G. d'Avino, P. Maffettone, F. Greco, and M. Hulsen, "Viscoelasticity-induced migration of a rigid sphere in confined shear flow," *Journal of Non-Newtonian Fluid Mechanics*, vol. 165, no. 9-10, pp. 466–474, 2010.

[25] H. Giesekus, "A simple constitutive equation for polymer fluids based on the concept of deformation-dependent tensorial mobility," *Journal of Non-Newtonian Fluid Mechanics*, vol. 11, no. 1-2, pp. 69–109, 1982.

[26] R. Bird, R. Armstrong, and O. Hassager, *Dynamics of polymeric liquids*. Wiley, 2nd ed., 1987.

[27] L. Derzsi, M. Kasprzyk, J. P. Plog, and P. Garstecki, "Flow focusing with viscoelastic liquids," *Physics of Fluids*, vol. 25, no. 9, p. 092001, 2013.

[28] A. Raisi, M. Mirzazadeh, A. S. Dehnavi, and F. Rashidi, "An approximate solution for the couette–poiseuille flow of the giesekus model between parallel plates," *Rheologica acta*, vol. 47, no. 1, pp. 75–80, 2008.

[29] B. Ho and L. Leal, "Migration of rigid spheres in a two-dimensional unidirectional shear flow of a second-order fluid," *Journal of Fluid Mechanics*, vol. 76, no. 4, pp. 783–799, 1976.

[30] K. Weissenberg, "A continuum theory of rhelogical phenomena," *Nature*, vol. 159, 1947.

[31] H. A. Barnes, J. F. Hutton, and K. Walters, *An introduction to rheology*, vol. 3. Elsevier, 1989.

[32] A. Naillon, C. de Loubens, W. Chèvremont, S. Rouze, M. Leonetti, and H. Bodiguel, "Dynamics of particle migration in confined viscoelastic poiseuille flows," *Phys. Rev. Fluids*, vol. 4, p. 053301, May 2019.

[33] F. Del Giudice, G. D'Avino, F. Greco, P. A. Netti, and P. L. Maffettone, "Effect of fluid rheology on particle migration in a square-shaped microchannel," *Microfluidics and Nanofluidics*, vol. 19, no. 1, pp. 95–104, 2015.

[34] M. Villone, G. D'avino, M. Hulsen, F. Greco, and P. Maffettone, "Particle motion in square channel flow of a viscoelastic liquid: Migration vs. secondary flows," *Journal of Non-Newtonian Fluid Mechanics*, vol. 195, pp. 1–8, 2013.

[35] P. Goswami, J. Chakraborty, A. Bandopadhyay, and S. Chakraborty, "Electrokinetically modulated peristaltic transport of power-law fluids," *Microvascular research*, vol. 103, pp. 41–54, 2016.

[36] P. Pranay, R. G. Henríquez-Rivera, and M. D. Graham, "Depletion layer formation in suspensions of elastic capsules in newtonian and viscoelastic fluids," *Physics of Fluids*, vol. 24, no. 6, p. 061902, 2012.

[37] S. Mukherjee, S. S. Das, J. Dhar, S. Chakraborty, and S. DasGupta, "Electroosmosis of viscoelastic fluids: Role of wall depletion layer," *Langmuir*, vol. 33, no. 43, pp. 12046–12055, 2017.

[38] R. G. H. Rivera, X. Zhang, and M. D. Graham, "Mechanistic theory of margination and flow-induced segregation in confined multicomponent suspensions: Simple shear and poiseuille flows," *Physical Review Fluids*, vol. 1, no. 6, p. 060501, 2016.

[39] N. Bressloff, M. Mansour, and C. Shearman, "Microvascular cell depletion model," in *World Congress on Medical Physics and Biomedical Engineering, September 7-12, 2009, Munich, Germany*, pp. 2095–2098, Springer, 2009.

[40] D. Quemada, "A rheological model for studying the hematocrit dependence of red cell-red cell and red cell-protein interactions in blood," *Biorheology*, vol. 18, no. 3-6, pp. 501–516, 1981.